**Title: Mechanosensitive dynamics of lysosomes regulates the emergence of leader cells during collective cell migration**

**Short title: Force-sensitive lysosome dynamics determines the leader cells**

Rituraj Marwaha[1,*], Simran Rawal[1,+], Purnati Khuntia[1,+], Manish Jaiswal[1], and Tamal Das[1,*]

1. Tata Institute of Fundamental Research Hyderabad (TIFR-H), Hyderabad – 500 046, India
[+]These authors have contributed equally
[*]All correspondence should be addressed to R.M. (Email: riturajmarwaha@tifrh.res.in) or T.D. (Email: tdas@tifrh.res.in).

**Keywords:** Collective cell migration, Leader cells, Lysosomes, Actin dynamics, Epithelial tissue, Mechanotransduction

## ABSTRACT

Collective cell migration during morphogenesis, cancer metastasis, and wound healing depends on the emergence of leader cells at the migration front. However, the cellular changes that enable only a few cells to become the leader cells, remain elusive. Here we show that the leader cells in *Drosophila* embryo and mammalian epithelial monolayer emerge through a mechanosensitive relocalization of lysosomes. Before the leader cells display their characteristic lamellipodial protrusions, lysosomes accumulate at their leading periphery. Promoting this lysosome accumulation augments the leader cell emergence, while inhibiting it suppresses the latter. Moreover, experiments modulating cellular forces by chemical inhibition, optogenetics, and micropatterning show that peripheral accumulation of lysosomes depends on the actomyosin contractility. Mechanistically, peripheral lysosomes associate with the inactive form of small RhoGTPase Rac1 and remove it from the vicinity of plasma membrane. Removal of inactive Rac1 molecules leads to an increased Rac1-activity at the leading periphery, triggering actin polymerization and lamellipodium formation. Taken together, lysosome appears as a unique intracellular platform that links mechanical and biochemical signals and thereby controls the emergence of leader cells. We, therefore, discover a previously unknown function of lysosome in collective cell migration, significantly expanding its scope in cell and developmental biology.

## SIGNIFICANCE STATEMENT

Leader cells have profound effects on the efficacy of wound healing, morphogenesis, and cancer metastasis. Yet, it remains intriguing how these special cells, with their remarkable lamellipodial protrusions, emerge from a seemingly homogeneous population. Here, using an interdisciplinary approach, which combines live-cell microscopy, optogenetic manipulation, and micropatterning, we discover that a cellular organelle, lysosome, changes its position in response to the cellular force-field and accumulates at the leading periphery of the emerging leader cells. In these cells, peripheral lysosome accumulation induces polymerization of actin cytoskeleton and formation of lamellipodial protrusions. Together, our results reveal a critical and unique role of lysosomes in collective cell migration, beyond the conventional reputation of this organelle as a cellular compartment dedicated for catabolism.

## INTRODUCTION

Collective cell migration is the coordinated movement of cells, which is essential for organogenesis, embryo development, wound healing, tissue regeneration, and cancer metastasis (1-14). For successful migration of epithelial cell collectives, a few cells at the migration front undergo phenotypic transformation to form distinct lamellipodial structures and emerge as

leader cells (1, 15). These cells provide guidance to collective cell migration (14, 16, 17) and are critical for epithelial wound healing (18, 19), branching morphogenesis (20, 21), and cancer metastasis (10, 22-24). In spite of this physiological importance, what factors selectively designate only a few cells at the migration front as the leader cells remains largely unknown. Nevertheless, there are evidences that both mechanical and biochemical cues might be influential here (25, 26). For example, the spontaneous fluctuations in the cell force-field, which is defined by the cell-cell and cell-matrix forces, influence the leader cell formation (25). Much before the leaders actually start showing their characteristic lamellipodial structures, elevated traction forces and tensile stresses appear behind the would-be leader cells (25). These results suggest a non-cell autonomous regulation of leader cell emergence. In addition to this mechanical regulation, spatial patterns of cellular signalling proteins such as p120-catenin (27), RhoA (26), and Notch-Dll4 (28) distinguish the leader cells from other non-leader cells at the migration front and the follower cells behind the leaders. In fact, intrinsic polarized activity of Rac and RhoA GTPases is an integral signature of leader cell emergence (26). Additionally, cues for leader cell emergence can also come from the extracellular milieu through the interaction of the migrating cells with the compliant extracellular matrix via focal adhesions (1) and with the soluble signalling via self-generated chemokine gradient (29). Moreover, a recent study has identified the tumour suppressor protein p53 as a key marker for leader cells (18). Elevated levels of p53 guides leader cell emergence and modulates p21-CDK pathway to regulate collective migration (18). But a connection between the mechanical cues and the biochemical events leading to leader cell emergence remains elusive.

As the sedentary cells becomes motile and develop a clear front-to-rear polarity, the intracellular organization undergoes a conspicuous transformation (1). This transformation requires both breaking of the existing structures and making of new structures. To understand that, previous studies have primarily focused on the dynamics of actin cytoskeleton during the emergence of leader cells. However, the role of other intracellular structures, including many cellular organelles, in this process remains unexplored. Relevantly, one may presume that lysosomes, which are crucial for catabolism and recycling of various biomolecules, might play a critical role in the cellular transformation to a motile state. Indeed, lysosomes can act as a signalling hub regulating cell growth, death, and differentiation (30). They also house various proteins which regulate cell adhesion (31, 32) and migration (33). At a single cell level, lysosomes regulate the dynamics of focal adhesions in migrating fibroblasts (32). Again, during dendritic cell migration, lysosomes accumulate in the direction opposite of migration and locally release calcium to modulate actomyosin dynamics supporting cell propulsion (34). Finally, lysosomes respond to mechanical properties of the extracellular matrix by altering their intracellular position (35). While it seems that lysosomes are capable of integrating mechanical signals and biochemical signals, very little is known about the specific roles of this organelle in collective cell migration. In this work, we explore the roles of lysosomes in the emergence of leader cells during collective cell migration.

## RESULTS

**Lysosomes accumulate at the leading periphery of the leader cells in *Drosophila* and in mammalian epithelial monolayer.** First, to study the dynamics of lysosomes during collective cell migration, we grew Madin-Darby canine kidney (MDCK) epithelial cells to confluence into the wells of a migration chamber (Supplementary fig. 1A). In this system, after lifting the confinement off, cells migrate as a two-dimensional epithelial sheet. We then fixed these cells at 0, 2, and 4 hours post-confinement lift off and immunostained them with antibodies against two lysosomal membrane markers, namely LAMP1 and LAMP2 (Supplementary fig. 1B). We observed that in the cells at the migration front (marginal cells), lysosomes accumulated at the cell periphery, whereas the cells in the follower layer did not show any change in lysosome localization (Supplementary fig. 1B). Interestingly, among the marginal cells, we observed

further enhanced lysosome accumulation at the leading periphery of the leader cells, which were marked by their extended lamellipodial structures (Fig. 1A). We subsequently computed the fraction of peripherally-localized lysosomes with respect to the total lysosome number in a cell and reported it as peripheral occupancy of lysosomes (POL) (Fig. 1B). A comparison of this quantity between leader and non-leader marginal cells revealed a significantly higher fraction of lysosomes localized to cell periphery in leader cells than in non-leader cells (Fig. 1C). To test the generality of our findings, we next repeated the aforementioned measurements in a murine mammary epithelial cell line, EpH4. Enhanced peripheral localization of lysosomes in leader cells emerged in this model as well (Supplementary figs. 1C-D). Finally, to check if this observation might be relevant to *in vivo* systems, we examined lysosome localization in a wound healing model in *Drosophila melanogaster* embryos (Figs. 1D-E and Supplementary fig. 1E). It is known that the epidermal wound closure in stage-15 *Drosophila* embryos occurs by a combination of pursed-string contraction of actin cables and lamellipodial crawling (36). We, therefore, used glass needles (0.5 µm inner diameter and 100 µm outer diameter) mounted on a femtojet microinjection system to create wounds in stage-15 embryos. Since the wound was sealed completely in 1-2 hours depending upon the size of the wound, we fixed these embryos at 15 minutes post-wounding, and stained them for lysosomes and actin (Fig. 1E and Supplementary fig. 1E). We subsequently observed emergence of lamellipodial structures in some of the cells at the migration front (Fig. 1E). At the same time, very similar to what we had observed in epithelial cell line, lysosomes accumulated at the periphery of these cells (Fig. 1E). These results suggested that lysosome accumulation at the periphery of leader cells might be evolutionary conserved.

Next, we asked whether peripheral accumulation of lysosomes in the marginal cells, including the leader cells, was a result of an increased lysosome biogenesis or of an escalated anterograde movement of the organelle. Considering that nuclear localization of Transcription Factor EB (TFEB) is an indicator of enhanced lysosome biogenesis (37, 38), we examined TFEB localization. However, we did not observe TFEB accumulation in the nuclei of marginal cells (Supplementary fig. 2A). We further quantified the number of lysosomes in the marginal and follower cells, before and during migration, and did not observe any significant change (Supplementary fig. 2B). These results eliminated the possibility of *de novo* lysosome biogenesis and pointed towards the polarized transport of lysosomes in leader cells. Since microtubules act as the track for bi-directional molecular motor-mediated transport of lysosomes, we envisaged that disrupting microtubules would abolish the dynamic peripheral accumulation of lysosomes. We, therefore, disrupted the microtubules by using nocodazole at a concentration (10 µM) that did not affect the collective migration of MDCK cells. Nocodazole treatment led to the loss of peripherally localized lysosomes (Supplementary fig. 2C-D), and at the same time, we observed a delayed emergence of leader cells upon nocodazole treatment. In this case, leader cells emerged only after 4 hours post confinement removal as compared to after 1-2 hours under the vehicle control condition (Supplementary fig. 2D). Moreover, downstream effectors of small GTPase Arl8b controls the lysosome movement on microtubule track. Among these proteins, lysosome adaptor protein SKIP recruits the plus-end directed kinesin motor to lysosome(39). We, therefore, hypothesized that transfecting the cells with a kinesin binding defective mutant of SKIP (SKIP WD->2XA) would provide more specific disruption of lysosome dynamics, without affecting the microtubule structure. Subsequently, SKIP mutant-expressing cells showed reduced peripheral accumulation of lysosomes (Supplementary Fig. 2E-F). These results collectively indicated that peripheral accumulation of lysosomes in marginal cells is the result of a dynamic localization process and is independent of lysosome biogenesis.

Finally, to understand how the lysosome dynamics is connected to actin dynamics in leader cells, we performed live-cell imaging of LifeAct-eGFP-expressing MDCK cells having Dextran-647 (Alexa fluor 647 labelled dextran) pre-labeled lysosomes (Fig. 1F and

Supplementary video 1). Lysosomes in these cells showed peripheral accumulation followed by dispersal, and subsequently, the lamellipodial protrusions started emerging (Fig. 1F and Supplementary video 1). Distance versus time plots for leaders and other non-leader marginal cells showed differential lysosome movement along the cell periphery (Fig. 1G). Further, live-cell imaging of LifeAct-expressing MDCK cells having Dextran-647 labeled lysosomes clearly show that lamellipodia extension happened in lysosome-rich zones (Figs. 1H-I and Supplementary video 2). In contrast, the actin structure was retracted from lysosome deficient regions (Figs. 1H-I and Supplementary video 2). Taken together these results show that lysosome accumulation at the cell periphery precedes the emergence of leader cells and is spatiotemporally correlated with the initiation and extension of lamellipodial structures in these cells.

**Peripheral accumulation of lysosomes is necessary for leader cell emergence.** Next, we sought to examine whether the peripheral accumulation of lysosomes is necessary for the emergence of leader cells. To this end, we hypothesized that if that was the case, preventing lysosome from moving to cell periphery would reduce the propensity of leader cell emergence. Conversely, forcing lysosomes to cell periphery would increase this propensity. To test these hypotheses, we first treated the MDCK epithelial monolayer with either Acetate Ringer's (AR) or Alkaline Ringer's (AlkR) solution for 30 minutes before the initiation of migration and let the cells migrate in presence of these solutions for 4 hours (Supplementary figs. 3A-C). AR solution promotes peripheral accumulation of lysosomes while AlkR solution promotes perinuclear accumulation(40). Using the time-lapse images recorded every 15 minutes, we analysed the number of leader cells emerging from migrating monolayers. Cells treated with AR with predominantly peripheral lysosomes displayed a significantly higher fraction of leader cell emergence than AlkR-treated cells with perinuclear lysosomes (Supplementary fig. 3D). These results suggested that propensity of leader cell emergence indeed depends on lysosome localization.

However, AR and AlkR solution impert global perturbation to lysosome distribution, which may have secondary effects on migration. Hence, to specifically modulate lysosome distribution in cells, we switched to a method that allowed us tweaking of lysosome localization in individual cells. To alter the organelle localization in a cell-specific manner, we resorted to the Reversible Association of Motor Protein (RAMP) system (41). In this system, interaction between streptavidin-bound to motor protein and streptavidin binding protein (SBP) fused to an organelle localizing protein drives the preferential localization of the target organelle. To this end, we first generated stable cell lines expressing streptavidin-bound to motor protein, mch-Kif5b*-Strep or Strep-Kifc1*-mch (Supplementary figs. 3E-F). mch-Kif5b*-Strep generates plus-end directed movement accumulating the target organelle at the cell periphery, while Strep-Kifc1*-mch generates minus-end directed movement accumulating the target organelle near the cell nucleus (Figs. 2A and 2C, respectively). Further, these cells were transiently transfected with LAMP-1-SBP-GFP, targeting lysosomes, and seeded in the migration chamber. By the interaction between Streptavidin and SBP, lysosomes are either localized to the cell periphery in mch-Kif5b*-Strep-expressing cells or to the perinuclear region in Strep-Kifc1*-mch-expressing cells (Figs. 2A and 2C). Using fluorescence time-lapse imaging, we then followed the LAMP1-SBP-GFP expressing cells at the migration front (Figs. 2B and 2D and Supplementary videos 3-4). Interestingly, the LAMP1-SBP-GFP-expressing cells in mch-Kif5b*-Strep background, which had peripherally localized lysosomes (Fig. 2E and Supplementary video 3), showed significantly increased propensity of leader cell formation than the LAMP1-SBP-GFP-expressing cells in Strep-Kifc1*-mch background (Fig. 2F and Supplementary video 4), which had lysosomes mostly localized to the perinuclear region (Fig. 2F). The probability of cells with peripheral lysosomes becoming leaders was 55% ± 3% (mean ± standard deviation), while same the probability of cells with perinuclear lysosomes was 7%

± 2% (Fig. 2G). Relevantly, the baseline probability is 16% ± 2% in control case (Supplementary fig. 3D), implying approximately one out of six marginal cells becomes the leader cells. Moreover, we found that cells co-expressing mch-Kif5B*-strep and LAMP1-SBP-GFP possessed prominent lamellipodial structures and mature focal adhesions perpendicular to the migrating front (Fig. 2H). In contrast, cells co-expressing Strep-KifC1*-mCh and LAMP1-SBP-GFP possessed peripheral actin cables and less prominent focal adhesions parallel to the migrating front (Fig. 2I). These results suggested that mch-Kif5B*-strep expression and subsequent peripheral localization of lysosomes promoted leader-like cell morphology, while mch-Kifc1*-Strep expression and subsequent perinuclear localization of lysosomes promoted follower-like cell morphology(25, 26). Finally, we obtained similar results using EpH4 cells, where cells transiently transfected with mch-Kif5B*-strep and LAMP1-SBP-GFP or Strep-KifC1*-mCh and LAMP1-SBP-GFP showed lamellipodium or actin cables, respectively (Supplementary Fig. 3G-H). In summary, we were able to regulate the propensity of leader cell emergence at the migrating front by altering lysosome localization. Collectively, these results suggested that peripheral localization of lysosomes is both necessary and sufficient for leader cell emergence.

**Forces generated by the actomyosin contractility alter lysosome localization**. In a cohesively migrating epithelium, leader cells emerge through an active mechanical process, where forces from cell-cell and cell-ECM interactions play critical roles (2, 4, 8, 42). We, therefore, asked whether the peripheral accumulation of lysosomes in leader cells might be mechanosensitive. To test this possibility, we reduced the actomyosin contractility by using a non-muscle myosin II inhibitor, blebbistatin and a Rho-associated protein kinase inhibitor, Y27632. We used sub-optimal concentrations of these drugs so that the cells were able to migrate (Fig. 3A). We pre-treated the cells for 30 minutes with the desired concentration of these inhibitors. We then lifted off the confinement and allowed the cells to migrate in a media containing these inhibitors. Subsequently, we observed reduced accumulation of lysosomes at the cell periphery upon drug treatment (Fig. 3B). In addition, there was no selective emergence of leader cells at the migrating front (Fig. 3A). This set of experiments provided the first evidence supporting the mechano-sensitivity of lysosome localization during collective cell migration.

To test the connection between the actomyosin contractility and the peripheral accumulation of lysosomes further, we next performed two independent sets of experiments. Previous studies had shown that increased traction forces and tensile stresses among the follower cells preceded leader cell emergence (25). This observation is connected to the fundamental premise of contact inhibition of locomotion (CIL), where one can imagine a leader-follower doublet to be a connected pair of cells experiencing a force perpendicular to the cell-cell contact(43, 44) (Supplementary Fig. 4A). Therefore, increased tension in one cell will trigger the formation of lamellipodium in the other cell, away from the first cell (Supplementary fig. 4A). Hence, we hypothesized that in such a cell-pair system, lysosomes would localize towards the cell periphery, away from the cell-cell interface. Moreover, this localization would depend on the actomyosin contractility. To test this hypothesis, we plated MDCK cells at a low density to allow them to form cell pairs and subjected them to overnight treatment with blebbistatin to reduce the actomyosin contractility (Supplementary Fig. 4B). As compared to the control, polarized localization of lysosome, away from the cell-cell interface, was lost in blebbistatin-treated cells, and lysosomes dispersed throughout the cell body (Supplementary Fig. 4B). To test whether lysosome polarization could be restored upon the revival of actomyosin contractility, we performed subsequent drug washout experiments. Cells maintained under drug-free condition for 4 hours partially regained the lysosome polarization (Supplementary fig. 4B). These results indicated that the force experienced at the cell-cell interface of a leader-follower pair is crucial for lysosome localization.

We further examined whether locally-enhanced cellular forces within an epithelial monolayer might be sufficient to induce lysosome polarization away from the interface. To this end, we used an Opto-GEF-based strategy (45) to enhance the actomyosin contractility of a specific cell within the monolayer (Fig. 3C). This experiment involved blue light-mediated photo-stimulation of cryptochrome 2 (CRY2)-bound catalytic domain of a RhoA-activator, ARHGEF11. CIBN, which is one of the binding partners of CRY2, was engineered to localize either at plasma membrane or at mitochondria. Upon photo-stimulation, CRY2-CIBN association triggered plasma membrane (Fig. 3C and Supplementary video 5) or mitochondrial localization (Supplementary Fig. 4C and Supplementary video 6) of the RhoA-activator. When localized to plasma membrane, RhoA-activator increased the actomyosin contractility(45). We used the mitochondrial localization of RhoA-activator as the negative control for this experiment. Subsequently, we hypothesized that enhanced contractility of a photo-stimulated cell would polarize the lysosomes in the neighboring cells, away from the former (Fig. 3C). As expected, upon photo-stimulation, lysosomes in the cells adjacent to the excited cell moved towards the cell periphery, away from the stimulated cell (Figs. 3D-E). But, in the negative control, where RhoA-activator localized to mitochondria, lysosomes in the cells adjacent to the stimulated cell did not undergo any such changes in localization (Supplementary figs. 4D). These two sets of experiments revealed how under the framework of CIL, mechanical forces transmitted through the cell-cell interface polarized lysosomes away from the interface. Lysosomes, therefore, appear as the missing cellular connection between increased forces among the follower cells and the emergence of leader cells.

Finally, we hypothesized that if the mechanical forces regulated peripheral lysosome localization during the emergence of leader cells, then any cue that spatially biases leader cell emergence should also spatially bias the peripheral localization of lysosomes. One such cue is the wound geometry. Having highly positive-curved beaks at the migration front leads to the emergence of leader cells at the tip of the beak, due to strong force concentration at those points (46-48). Would such beaks show enhanced peripheral localization of lysosomes? To answer this question, we used a micropatterning approach to fabricate silicone stencils made of polydimethylsiloxane (PDMS). These stencils would create wounds with a single beak to allow one or two cells to have the geometrical cue to become the leader cells (Fig. 3F and Supplementary fig. 4E). We then seeded cells in these micropatterned chambers, labelled lysosomes using Dextran-647, lifted off the confinement, and performed live-cell imaging. Upon lifting the stencil, we indeed observed enhanced lysosome accumulation at the tip of these beaks as compared to their sides (Figs. 3G-H and Supplementary video 7). At the same time, lamellipodial structures emerged out of the beak region while actin fibers ran along both sides (Fig. 3G). These results suggested that the spatial concentration of mechanical force in the epithelial monolayer correlates with the enhanced peripheral localization of lysosomes, strengthening the premise of mechanosensitive localization of lysosomes during leader cell emergence. It also strengthened the aforementioned correlation (Fig. 1H) between peripheral localization of lysosomes and lamellipodia formation through the modification of actin cytoskeleton.

**Inactive Rac1 GTPase localizes to lysosomal membranes.** We then asked how the peripheral localization of lysosomes promotes the lamellipodia formation by locally modifying the actin cytoskeleton. In migrating epithelial cells, actin dynamics depends on the localization and activation of small Rho GTPases, including Rho, Rac1, and Cdc42 (1, 9, 26, 49). These proteins switch between GTP-bound active state and GDP-bound inactive state. To identify if any form of these three small Rho GTPases interacted with lysosomes, we conducted a screen using the constitutively active (CA) and dominant-negative (DN) forms of these GTPases (Figs. 4A-C and Supplementary figs. 5A-D). These proteins were also tagged with a fluorescent protein for visualization. CA and DN represented the active and inactive state of the small Rho GTPases,

respectively. We transfected MDCK cells with one of the forms, grew these cells under confinement, and lifted off the confinement to allow them to migrate for 4 hours. We then fixed and immunostained these cells to visualize lysosomes (Figs. 4A-C and Supplementary figs. 5A-D). To our interest, we observed that out of these six proteins, only the dominant-negative form of Rac1 GTPase (Rac1-DN) colocalized with the lysosomal marker LAMP1 (Fig. 4B). Other Rho family GTPases did not show any appreciable colocalization with lysosomes (Supplementary figs. 5A-D). Also, the wildtype (Rac1-WT) and Rac1-CA were primarily plasma membrane-localized whereas Rac1-DN was distributed on lysosomes and at plasma membrane in both MDCK and EpH4 epithelial cells (Fig. 4A-C and Supplementary figs. 4E-G). Mander's coefficient analysis between Rac1-WT, Rac1-CA, and Rac1-DN with the lysosomal membrane marker LAMP1 confirmed this localization pattern (Fig. 4D and Supplementary fig. 5H). With these results, we wondered whether lysosomes are capable of scavenging Rac1-DN. To reveal the dynamic association between lysosomes and Rac1-CA or Rac1-DN, we used a photoconversion strategy. In this strategy, we expressed either mEos-Rac1-DN or mEos-Rac1-CA in MDCK cells having lysosomes labeled with Dextran-647. Upon photoconversion using 405 nm illumination, the emission spectrum of mEos fluorescent protein shifts from green to red, allowing us to visualize the dynamics of the protein of interest. In this experiment, we allowed mEos-Rac1-DN or mEos-Rac1-CA transfected cells to migrate, and during migration, we photoconverted the colour of mEos proteins near the growing lammellipodial protrusions using 405 nm light. We then tracked the photoconverted proteins for their redistribution within the cell (Figs. 4E-H). As depicted by kymographs, live-tracking revealed puncta formation events for photoconverted mEos-Rac1-DN. Interestingly, these punctate structures merged with lysosomes positioned nearby, showing significant colocalization between the two (Fig. 4F and Supplementary video 8). In contrast, photoconverted mEos-Rac1-CA diffused throughout the plasma membrane, and puncta formation was negligible in this case (Fig. 4H and Supplementary video 9). Collectively, these results indicated that lysosomes have a specific affinity for scavenging only the inactive form of Rac1, which piggybacks on the lysosomal membrane and move away from the plasma membrane (Figs. 4E-H). These results also suggested that the presence of lysosomes at the cell periphery should lead to an increased Rac1 activity, leading to branched actin polymerization and lamellipodium formation (Figs. 1F-I). To test this prediction, we measured the peripheral Rac1-activity with a FRET-based Rac1 sensor (49) in presence or absence of AR solution, which promotes peripheral accumulation of lysosomes (40). This experiment yielded two key results. First, the basal level Rac1 activity in quiescent cells (T= 0) increased upon AR-treatment (Figs. 4I-J, *left panels*). Second, although there was an increase in Rac1 activity during the cell migration even in absence of AR-treatment, upon AR-treatment, we observed further increase in Rac1 activity (Figs. 4I-J, *right panels*). In addition, upon AR-treatment, many migrating cells showed unusual projections throughout the cell periphery (Fig. J, *right panels)*. Taken together, these results suggested that the peripherally-localized lysosomes promoted Rac1 activity (Fig. 4K), thus linking the force-induced peripheral accumulation of lysosomes to lamellipodium formation in the emergence of leader cells during collective cell migration (Fig. 5)

## DISCUSSION

Ever since Edward Ruth published his pioneering study on epithelial wound closure using the fragments of frog skin (50), the ubiquity and importance of leader cells in collective cell migration have become apparent in various physiological contexts (1, 10, 15, 18, 22). Yet, for more than a century, it has remained intriguing how these special cells, with their characteristic lamellipodial protrusions, emerge from a seemingly homogeneous population. Once the free-edge is generated by wounding, cells at the wound margin experience an asymmetry. While cells within the epithelium are encircled by neighbouring cells from all sides, cells at the

migration front have at least one cell-free edge. Consequently, the geometric, physical, and molecular asymmetry arising at this free edge creates a spontaneous cue for polarized activation of small Rho GTPases, whose activity would otherwise be restricted by cell-cell junctions. In fact, asymmetric spatiotemporal regulation of Rho GTPases, including Rac1, is central to forming actin projections and stress fibres during collective cell migration, especially in the emergence of leader cells (1). However, this asymmetry is equally likely to generate lammellipodial structures in all cells at the migration front, and it is not obvious at what level the selection of a leader cell is decided. Previous experiments have shown that leader cell emergence is not an entirely stochastic biochemical event, as conventionally believed. Instead, the localization of highly tensile peaks in the stress landscape determines the precise location of the leaders. These experiments have also suggested that enhanced tensions at the cell-cell junction promote formation of lamellipodial protrusions away from the leader-follower interface, towards the cell-free space, in accordance with the fundamental principles of contact inhibition of locomotion (43, 44) (Supplementary fig. 4A). However, what has remained elusive is the connection between this biophysical driving force and the eventual activation of Rac1 leading to lammellipodia formation. It was, therefore, not clear how these biophysical and biochemical paradigms can be unified under a single mechanistic framework.

The present study identifies lysosomes as an intracellular platform linking mechanical and biochemical signals towards the regulation of leader cell emergence. At one end, lysosomes respond to changes in the force landscape of the emerging leaders by localizing to the cell periphery (Fig. 5). At the other, they transiently colocalize with the inactive form of small GTPase Rac1. This specific lysosome-Rac1 interaction supports lamellipodia formation by shuttling the inactive form of Rac1 away from the plasma membrane. This process shifts the balance in favour of actin crosslinking to form migratory lamellipodial structures (Fig. 5). Thus, lysosomes sense local force field and regulate lamellipodia formation by modulating the Rac1 signalling. Lysosomes are dynamic organelles that move bidirectionally on microtubules. Previous studies have shown that the position of lysosomes is critical for their function(33). Here, we elucidate how lysosome relocalization inside a cell at the migrating front determines the probability of that cell emerging as a leader cell, by a novel mechanism involving lysosome-Rac1 interaction. Next, it will be interesting to probe how lysosomes influence the dynamics other factors, including p53 (18) and Dll4 (28), in the context of leader cell emergence. Also, the underlying mechanism that makes lysosome mechanosensitive, needs to be elucidated.

Relevantly, Rac1 molecules organize into nanoclusters at the plasma membrane and form a gradient of spatial signalling. Rac1 is known to stay active for a few minutes in migrating cells (51, 52). We speculate that lysosomes shuttling the inactive Rac1 away from the site of growing lamellipodia are essential for maintaining greater pools of active Rac1, which can further recruit actin remodeling proteins such as Arp2/3 and WAVE. A previous work (53) has shown that early endosomes act as sites for Rac1 activation and transport activated Rac1 to the plasma membrane during single-cell migration. It will be interesting to explore the cross-talk between lysosomes and early endosomes to further characterize the signalling pathways underlying leader cell formation during epithelial migration (9). Finally, the coherent observation of lysosome accumulation in the leader cells of mammalian epithelial monolayer and *Drosophila* epidermis indicates that the process we discovered could be evolutionary conserved in epithelial wound healing. However, it remains unknown whether lysosome-Rac1 interaction is also critical for other kinds of single and collective cell migrations (2), including neural crest cell migration in vertebrates (2), border cell migration in *Drosophila* (9), and collective migration of lateral line primordial cells in Zebrafish (54). In addition, given that lysosomes play an important role in the continuous cross-layer migration and differentiation of keratinocytes within a mammalian epidermis (55), lysosome-Rac1 signalling axis might be critical for the development and maintenance of the multi-layered epidermal epithelium. Collectively, the results of our experiments and their implications place the functioning of

lysosomes at a crucial junction of mechanochemical signals during collective cell migration and uniquely expand the scope of this organelle beyond its conventional role in the catabolism of cellular materials.

## MATERIALS AND METHODS

**Cell culture**. Madin-Darby canine kidney (MDCK) and EpH4-Ev epithelial cells were used in this study. Tetracycline-resistant wild-type MDCK (MDCK-WT) cell line was a gift from Yasuyuki Fujita. MDCK cells were cultured in Dulbecco's modified Eagle's medium (DMEM) supplemented with GlutaMax (Gibco) with 5% foetal bovine serum (tetracycline-free FBS, Takara Bio) and 10 U $mL^{-1}$ penicillin and 10 µg $mL^{-1}$ streptomycin (Pen-Strep, Invitrogen) in an incubator maintained at 37°C and 5% $CO_2$, unless mentioned otherwise. Eph4-Ev cells (ATCC; CRL-3063) were cultured in Dulbecco's modified Eagle's medium supplemented with GlutaMax (Gibco) with 10% foetal bovine serum (tetracycline-free FBS, Takara Bio) and 1.2 µg ml−1 puromycin (Gibco) in an incubator maintained at 37 °C and 5% CO2.

MDCK cells stably expressing mCherry-Kif5b*-Strep and Strep-KifC1*-mCherry, cells were transfected with the respective plasmids using Lipofectamine2000 (Invitrogen) following the manufacturer's instructions. 16-18 hours post-transfection, cells were seeded via serial dilution in a 96-well plate, such that each well had a single cell. Forty-eight hours post-cell seeding, the cells were subjected to selection media (DMEM-GlutaMax plus 5% FBS) containing 400µg $mL^{-1}$ of Geneticin (Invitrogen). The growth of single cell-derived colonies was monitored over two weeks, following fluorescence confirmation. Colonies with a homogenous expression of the fluorescently tagged protein of interest were expanded and further maintained in 100µg $mL^{-1}$ Genetic containing media. All transient transfections were done using Lipofectamine2000 following the manufacturer's protocol.

Cell migration assays were performed using adhesive biocompatible silicone culture inserts from iBidi. 5 x $10^4$ cells suspended in an 80 µL cell culture medium were seeded in a culture insert stuck to glass-bottom dishes and incubated at 37°C in a 5% $CO_2$ humidified chamber. After 18 hours of cell seeding, the cells form a monolayer, and the culture insert is lifted to allow the cells to migrate. All migration experiments were carried out at 37°C and in a 5% $CO_2$ humidified chamber.

***Drosophila melanogaster* embryo microinjection wounding assay**. All flies were maintained at 25°C on a 12h diurnal cycle. Wildtype flies (CANTON-S) were used for in vivo wound assay. Drosophila melanogaster embryo wounding assay was performed as described earlier (56). Briefly, stage 15 embryos were collected on grape juice plates and were transferred to collection tubes with the help of a fine paint brush and water. The embryos were subjected to bleach treatment for 2 minutes for dechorination followed by 10 water washes and then tap dried them on a paper towel. The embryos were then transferred to an agar plate and aligned such that they are at right angle to the microinjection needle. Glass slide with double sided tape was used to transfer the embryos for microinjection. Air dried the embryos for approximately 5-7 minutes and then applied halocarbon oil (Halo700). The slide with embryos was placed on the microscope, focused in line with the microinjection needle attached to an Eppendorf FemtoJet system. The microinjection needle was pierced through the embryos and allowed 15 minutes for wound closure at room temperature.

For fixation and immunostaining a previously described protocol was followed(57). Briefly, drain halocarbon oil from the slide and flush it with heptane to release the embryos from the double sided tape. Add 0.8ml 4% Formaldehyde prepared in PBS to a fresh tube and transfer embryos with heptane to this tube followed by rotation on an orbital shaker for 25 mins. Remove the aqueous solution from the bottom of the tube and followed by removing heptane. To devitellinize the embryos, rapidly add heptane followed by adding double to triple volume of 90% ethanol and mixing it vigorously by vortexing. Proceeded with embryos that settle down

in the tube. The embryos were given 5 quick washes with 1X PBS and then blocked in PBS+0.3%Triton-X100+0.5%BSA (PBTB) for 30 minutes at room temperature. Primary antibody LAMP (Abcam) was prepared in PBTB and embryos were incubated overnight at 4°C followed by three washes done in PBS+0.3%TritonX-100 (PBT). Secondary antibody was prepared in PBTB and incubated for 2 hours at room temperature followed by 5 washes with PBT. DAPI and Phalloidin staining was done along with the secondary antibody. The embryos were mounted in Fluoromount (Sigma) on a glass slide and imaged using confocal microscopy.

**Immunofluorescence**. Cells were fixed in 4% formaldehyde diluted in 1X PBS for 15 minutes at room temperature. For most antibody staining, cells were permeabilized with 0.25% TritionX-100 in PBS for 10 minutes at room temperature followed by three quick washes with 1X PBS to remove the detergent. Cells were treated with blocking/staining solution (0.1% TritonX-100in 1X PBS + 2% BSA) for 1 hour at room temperature, washed thrice with 1X PBS, and further incubated with primary antibody prepared in blocking solution for 2 hours at room temperature. Post-primary antibody incubation cells were washed thrice with 1X PBS and incubated with secondary antibody, DAPI, and Phalloidin dilutions prepared in the blocking/staining solution for 1 hour at room temperature. Finally, the samples were given 2 quick and a 5 minutes wash with 1X PBS before proceeding for confocal microscopy.
For staining LAMP1 (Abcam), cells were incubated with a blocking solution (0.2% Saponin+5%BSA in 1X PBS) for 30 minutes at room temperature followed by three washes with 1X PBS. Cells were incubated with the primary antibody in staining solution (PBS+0.2%Saponin) for 2 hours at room temperature, washed thrice with 1X PBS and further incubated for 1 hour with secondary antibodies, DAPI (4′,6-diamidino-2-phenylindole, 1μg $mL^{-1}$ in PBS) and Phalloidin made in staining solution. Cells were washed thrice with 1X PBS and imaged using confocal microscopy.

**Lysosome labelling for live cell imaging.** Lysosomes of MDCK cells for live-cell imaging experiments were labeled with Alexa-fluor conjugated 10,000 MW Dextrans (Dextran-647 from Invitrogen). Briefly, cells were incubated with Dextran-647 at a final concentration of 0.25mg ml−1 in complete media for 6 hours at 37 °C in a 5% CO2 humidified chamber. Media for cells was then replaced with complete media and incubated for another 12 hours to completely chase Dextran-647 to lysosomes.

**Confocal Microscopy.** Fluorescence images were acquired using 60X oil objective (PlanApo N 60x Oil, N.A=1.42, Olympus) and 100X oil objective (UPlanSApo, 100X/1.40 oil) mounted on an Olympus IX83 inverted microscope equipped with a scanning laser confocal head (Olympus FV3000). Time-lapse images of live samples were done in the live-cell chamber provided with the microscopy setup.

Photoconversion studies were done using MDCK cells that had been transiently transfected with mEos-Rac1 DN or mEos-Rac1 CA. Transiently transfected cells were seeded in culture inserts and proceeded for lysosome labeling using Dextran-647 as described above. Cells were allowed to migrate for 60 minutes to allow for lamellipodia formation in migrating cells Stimulation was done on a point region of interest juxtaposed to the site of growing lamellipodia using a 405nm laser at 2% intensity, looped over 25 times with a scan speed of 1000 μs/pixel. This was followed by LSM imaging of the green and red channels and Rac1 dynamics were tracked for 5 minutes.

Photoactivation experiment was carried out using 60X oil objective (PlanApo N 60x Oil, N.A=1.42, Olympus) mounted on an Olympus IX83 inverted microscope equipped with a scanning laser confocal head (Olympus FV3000), supported with live-cell imaging setup. 20 mM HEPES (Gibco) was used to maintain CO2 levels. MDCK cells expressing *optoGEF-RhoA* and *CIBN-GFP-CAAX* or *optoGEF-RhoA* and *Mito-CIBN-GFP* (control)(45), stained with

lysosomal marker Dextran-647 were used for the experiment. Pulse activation (20 iterations) was performed in the selected rectangular ROIs (whole cell or cell-cell junction) using a 488 nm laser with 2.0 % laser intensity at 4.0 µsec/pixel scan rate. Immediately followed by time-lapse (15 minutes, 30-sec interval) LSM imaging in 561 nm and 647 nm channels, to visualize RhoA activation and monitor lysosomal movement, respectively.

**Förster resonance energy transfer (FRET)-based Rac1-activity measurements.** FRET experiments for the Rac1 activity sensor were carried out in the live-cell confocal setup (Olympus FV3000). MDCK cells were first plated in a 24-well plate and transiently transfected with Rac1 sensor plasmids(49). After 6 hours, cells were trypsinized and seeded in migration chambers and left overnight to settle and form confluent monolayers in the chamber. Cells were simultaneously labeled for lysosomes using dextran-647. Control and AR treatment was given to cells as described in the Global perturbation of lysosome positioning using Ringer's solution method section. The images were acquired for control and AR-treated cells just after lifting off the confinement (T-0) and post 2 hours of migration (T-2 hours). The exposure times for donor, acceptor, and FRET channels were kept constant. Images of dextran-647 labeled lysosomes were also acquired. Each field yielded three 800 x 800-pixel images representing donor, acceptor, and FRET channels. Images were analyzed using custom software written in MATLAB (Mathworks).

**Inhibition studies.** For all inhibition studies, cells were pre-treated with the desired concentration of the inhibitor in opti-MEM for 30mins at 37°C in a 5% CO2 humidified incubator, before lifting the confinement/culture insert. During migration post removing the confinement, cells were kept in complete media containing the inhibitor at a given concentration for the required time. Actomyosin contractility was altered using Blebbistatin (Simga), a myosin inhibitor and Y27632 (Sigma), ROCK inhibitor at concentrations 5 µM and 30 µM respectively for MDCK cells. For microtubule disruption in MDCK cells, Nocodazole (Sigma) was used at 10µM. Cells were fixed and immunostained for the desired antibodies post inhibitor treatment.

**Global perturbation of lysosome positioning using Ringer's solution.** Lysosome positioning in MDCK cells was altered by subjecting cells to variants of Ringer's solution as described previously(40). Cells were incubated with either acetate Ringer's solution (80 mM NaCl, 70 mM sodium acetate, 5 mM KCl, 2 mM $CaCl_2$, 1 mM $MgCl_2$, 2 mM $NaH_2PO_4$, 10 mM HEPES, and 10 mM glucose, final pH 6.9) or Alkaline Ringer's solution (155 mM NaCl, 5 mM KCl, 2 mM $CaCl_2$, 1 mM $MgCl_2$ , 2 mM $NaH_2PO_4$, 10 mM HEPES, 10 mM Glucose, 0.5 mg $mL^{-1}$ BSA and 20 mM $NH_4Cl$) for 30 minutes before lifting the culture insert. After lifting the confinement the cells were allowed to migrate in either Acetate Ringer's or Alkaline Ringer's and migration was followed up to 4 hours. Control cells migrated in the presence of Opti-MEM, which has a pH of 7.2, and its composition overlaps with that of Ringer's solution. Cells were live imaged using 20X objective on Leica DMI8 inverted microscope using Leica Application Suite X (LAX, v3.7.0.20979) under different treatment conditions.

**Plasmids and Antibodies.** Source and dilution information for all primary and secondary antibodies used in immunofluorescence staining are given in Supplementary Table 1. Details of plasmids used in this study are listed in Supplementary Table 2 with their source.

**Micropatterning.** PDMS stencils with pillars of defined shapes were created using soft photolithography. Briefly, 150 um thick SU-8 2075 (Kayaku advanced materials, Y111074) was coated on a silicon wafer followed by soft baking at 65° C for 5 mins and 95° C for 20 mins. SU-8 was exposed in the desired pattern using the MicroWriter ML 3 Pro (Durham Optics

Magneto Ltd) followed by post-exposure baking at 65° C for 7 mins and 95° C for 15 mins. The unexposed photoresist was removed by immersing the wafers in the SU-8 developer (Kayaku advanced materials, Y020100) for 8-10 mins. Patterned SU-8 wafers were then hard-baked at 170° C for 45 mins. PDMS (Sylgard 184, Dow Corning) was mixed in a ratio of 1:10, degassed, and poured over the patterned wafers. After curing at 85 °C for 2 h, stencils with pillars were peeled off. The stencils were then treated with 2% Pluronic acid for 2 hrs followed by 15 mins of 1X PBS wash. PDMS stencil and a petri dish were plasma cleaned for 10 seconds and the stencil was then placed upon the dish. Cells were seeded around the pillars, and after confluence, the stencils were removed allowing the cells to migrate into the gaps.

**Image Analysis.** All image analysis for this study was performed using Fiji. peripheral lysosome occupancy (POL) was measured for cells at the margin of a migrating collective. The ROI box with a fixed width of 2.5 μM from the cell edge facing the gap was drawn over the cell of interest. The box was duplicated for the lysosome channel and a threshold was established to mark lysosomes. Using the Analyze Particles tool of Fiji the count of lysosomes was determined. For each cell, the total number of lysosomes was also calculated by manually marking the cell of interest and following the same approach as mentioned above for lysosome number calculation in the ROI. For calculating the POL, the number of lysosomes in ROI was divided by the total number of lysosomes in that cell. 20 marginal and leader cells per experiment were quantified from three independent experiments.

To measure POL for experiments involving OptoGEF-RhoA, cells adjoining the photoactivated cell were marked manually. The image was duplicated for the lysosome channel and subjected to thresholding to mark the organelle. Total number of lysosomes were manually counted. This was followed by marking the cell periphery of the same cell by using the Edit → Selection → Enlarge tool of Fiji to reduce the outline by 2.5 μm. Using the Edit → Clear tool the lysosomes in the perinuclear region were omitted and the remaining lysosomes in the cell periphery were counted manually. To get the POL for cells, the number of peripheral lysosomes was divided by the total number of lysosomes for each cell.

Colocalization analysis of different forms of small GTPase Rac1 with lysosomal marker LAMP1 was performed using the JACoP tool of Fiji. For measuring Mander's coefficient, cytoplasmic expression was analyzed by marking the cell boundary using a freehand tool in Fiji. The cytoplasmic Rac1 expression includes its vesicular component and its co-localization with lysosomes was measured. Analysis was performed for three independent experiments and 20-25 cells per transfection per experiment were analyzed.

**Statistical analysis.** Statistical analyses were carried out in GraphPad Prism 9. Statistical significance was calculated by Unpaired t-test with Welch's correction as mentioned in the corresponding figure. Scatter-bar plots were displayed as mean ± s.e.m. p-values greater than 0.05 were considered to be statistically not significant. No statistical methods were used to set the sample size. Quantification was done using data from at least three independent biological replicates. For analysis involving live-imaging experiments, data were collected from three independent experiments. All the experiments with representative images were repeated at least thrice.

## FIGURE LEGENDS

**Figure 1: Lysosome accumulation to the cell periphery in leader cells emerging from collectively migrating epithelial cells.**

**A**) Representative images of migrating monolayer of MDCK cells fixed at T-0 and T-2hrs post lifting off the confinement. Cells are immunostained for lysosomes using Anti-LAMP1, Alexa-fluorophore conjugated phalloidin labels actin, and DAPI marks the nucleus. **B**) Schematic representation of Peripheral/marginal occupancy of lysosome analysis, which measures

peripheral lysosome accumulation. **C**) Scatter column plot showing POL for marginal and leader cells at T-0 and T-2hrs in MDCK cells (n=3, 15 cells analyzed per cell type per experiment). Statistical significance was assessed using unpaired Student's *t*-test with Welch's correction (two-tailed). **D**) Diagram representing stage-15 *Drosophila melanogaster* embryo wounding assay. **E**) Confocal micrographs of wound closure in *Drosophila melanogaster* embryos fixed 15mins post wounding and immunostained with Anti-LAMP. Alexa-fluorophore conjugated phalloidin stains actin, and DAPI marks the nucleus. **F**) Live-imaging snapshots of actin and lysosome (labeled using Dextran-647) dynamics in LifeAct-GFP MDCK cells. The red arrowhead marks an emerging leader cell, and the cyan arrowhead marks a non-leader marginal cell. **G**) Kymographs showing differential lysosome dynamics in leader cell and non-leader marginal cell marked by red and cyan arrowheads respectively in F). **H**) Live imaging snapshots of lamellipodial and lysosome dynamics in a leader cell. White and yellow arrowheads mark lysosome-rich and deficient zones within a leader cell. **I**) Time vs. Distance plots showing growing lamellipodia in lysosome rich zone (1) and retraction of the actin structure in lysosome deficient region (2). Scale bar-10µm; **** denotes p-value<0.0001, n.s is not significant.

**Figure 2: Peripheral lysosomal bias leads to enhanced leader cell emergence in collectively migrating epithelia.**

**A and C**) Schematic depicting molecular basis and lysosome positioning outcomes using the RAMP (Reversible Association of Motor Protein) system. **B**) Representative fluorescence/ bright-field time-lapse imaging snapshots of MDCK cells expressing mCherry-Kif5B*-Strep transiently transfected with LAMP1-SBP-GFP. Pink arrowheads mark cells with co-expression of the two plasmids. **D**) Representative time-lapse imaging snapshots of MDCK cells expressing Strep-KifC1*-mCherry transiently transfected with LAMP1-SBP-GFP. Pink arrowheads mark cells with co-expression of the two plasmids. **E-F**) MDCK cells co-expressing either mCherry-Kif5B*-Strep (E) or Strep-KifC1*-mCherry (F) and LAMP1-SBP-GFP were fixed 4hrs post-migration and stained for actin and nucleus using Alexa-fluorophore conjugated phalloidin and DAPI respectively, further imaged using a confocal microscope. Cells with peripheral lysosomes (E) form extended lamellipodia, and cells with perinuclear lysosomes have actin cable. **G**) Graph representing the percentage of leader cells emerging in case of cells co-expressing mCherry-Kif5B*-Strep or Strep-KifC1*-mCherry and LAMP1-SBP-GFP, allowed to migrate for 4hrs, calculated as a fraction of co-transfected cells at the margin showing lamellipodial formation to the total co-transfected cells at the migration margin (n=3, 40-50 co-transfected cells per transfection combination per experiment were counted). **H-I**) Representative confocal micrographs of MDCK cells co-expressing either mCherry-Kif5B*-Strep (H) or Strep-KifC1*-mCherry (I) and GFP-LAMP1-SBP and immunostained for focal adhesions using anti-Paxillin. Actin was labeled using Alexa fluorophore-conjugated phalloidin, and DAPI marks the nucleus. Scale Bar-10µm. **** signifies p-value < 0.0001

**Figure 3: Actomyosin contractility drives peripheral localization of lysosomes.**

**A**) Control (DMSO), Blebbistatin (5µM), and Y27632 (30µM) treated MDCK cells were allowed to migrate for 2hrs, fixed, and stained for lysosomes (anti-LAMP2), actin(Phalloidin) and nucleus (DAPI). Images were acquired on a confocal microscope. **B**) Graph representing POL analysis for Control, Blebbistatin, and Y27632 treated MDCK cells (n=3; 20 cells per treatment per experiment). **C**) Diagrammatic representation of optogenetic control of Opto-RhoAGEF which allows to manipulate cell contractility and epithelial monolayer force landscape. Changes in lysosome distribution were recorded in cells juxta-positioned to the transfected and optogenetically altered cell. **D**) Live images of cells with Dextran-647 labeled lysosomes and expressing Opto-RhoAGEF (marked with cell boundary). Post activation with 488nm laser illumination, lysosome distribution was observed in the neighboring cell marked

by a yellow asterisk. White arrowheads mark lysosomes redistributing to cell periphery. **E**) POL analysis for pre-activation and post-activation of Opto-RhoAGEF (n=3; 12 cells analyzed). **F**) Schematic representing micropatterned single beak mold used for defining leader cell-like characteristics in select cells. **G**) Dynamics of dextran-647 labeled lysosomes were observed in LifeAct-GFP MDCK cells seeded in micropatterned chambers. Cells were allowed to migrate for up to 3hrs post lifting off the confinement. **H**) Graph representing POL calculated for non-leader marginal and leader cells (n=3; 10 cells analyzed). Scale bar-10µm; * , *** and **** signifies p-value<0.05, <0.001 and <0.0001 respectively.

**Figure 4: Peripheral lysosomes sequester inactive Rac1 from sites of growing lamellipodia.**

**A-C**) Representative confocal micrographs of MDCK cells transiently transfected with GFP-Rac1 WT, DN (dominant-negative; inactive form), and CA (constitutive active: active form), respectively, and allowed to migrate for 4hrs, followed by fixation and immunostaining for lysosomal markers LAMP1 and LAMP2. **D**) Colocalization of Rac1 WT, DN, and CA forms were assessed with LAMP1 by measuring Mander's coefficient (n=3, 25cells per transfection per experiment were analyzed). **E**) Photoconversion of mEos-Rac1DN to track its localization dynamics. MDCK cells transiently transfected with mEos-Rac1DN and dextran-647 labeled lysosomes were allowed to migrate for 60mins before photoconversion to initiate lamellipodia formation. Dynamics of Rac1DN puncta formation and trajectory were followed for photoconverted mEos-Rac1DN. **F**) Kymograph representing the colocalization dynamics of lysosomes and photoconverted mEos-Rac1DN. **G**) Photoconversion of mEos-Rac1CA to track its localization dynamics. Similar to mEos-Rac1DN, mEos-Rac1CA was photoconverted post 60mins of migration, and its dynamics and colocalization with dextran-647 labeled lysosomes were recorded. **H**) Kymograph representing distribution dynamics of lysosomes and photoconverted mEos-Rac1CA. No overlap observed for lysosomes and mEos-Rac1 CA. **I-J**) Representative heat maps of FRET-based Rac1 activity sensor and their corresponding confocal micrographs for Control or Acetate Ringer's treated MDCK cells. Cells were allowed to migrate for 2hrs. Lysosomes distribution was observed by labeling with Dextran-647. White arrowheads mark multiple cell protrusions observed upon Acetate Ringer's treatment. **K**) Mean FRET index was calculated for Control and Acetate Ringer's treated cells at T-0 and T-2hrs and represented as a scatter column graph. Scale bar-10µm; *, ** and **** signifies p-value < 0.05, 0.01 and 0.0001 respectively.

**Figure 5: Role of lysosomes in regulating leader cell emergence**

As epithelial cells start migrating collectively, lysosomes in the cells at the migration front start accumulating to the cell periphery in the direction of migration (**A**). Two hours into migration, leader cells start emerging from the cell collective. As some cells emerge as leaders, lysosomes in these cells show significantly higher accumulation of lysosomes to the periphery. Disruption of peripheral lysosomal pool severely reduces leader cell emergence. The cue for peripheral distribution of lysosomes comes from the mechanical forces experienced by and emerging leader cell. Forces generated at the cell-cell and cell-surface interface are translated to changes in actomyosin contractility within a leader, which guides the peripheral accumulation of lysosomes (**B**). Lysosomes in leader cells regulate the growth of lamellipodium by shuttling the inactive Rac1 away from the plasma membrane, thus shifting the balance towards active Rac1 which further regulates formation of actin crosslinks required for lamellipodial extension (**C**).

## AUTHOR CONTRIBUTIONS

R.M. and T.D. formulated the project. R.M. performed majority of the experiments and analysis. S.R. exclusively performed and analyzed micropatterning experiments and contributed to other experiments as well. P.K performed and analyzed opto-GEF

experiments. M.J. provided critical inputs to the design of *Drosophila* embryo experiments. R.M. and T.D. wrote the manuscript. M.J. edited the manuscript. All authors agreed on the manuscript as in the submitted version.

**ACKNOWLEDGEMENT**

We thank Ullas Kolthur and CCD lab members for critical discussion. R.M is grateful to Praver Gupta for his critical inputs on POL analysis. T.D. is a DBT/Wellcome Trust India Alliance intermediate fellow and partner group leader of the Max Planck Society (MPG), Germany. R.M. is a DBT/Wellcome Trust India Alliance early career fellow. Authors sincerely acknowledge generous funding from the DBT/Wellcome Trust India Alliance (Ref. No. IA/E/19/1/504967 to R.M. and IA/I/17/1/503095 to T.D.), partner group grant of the Max Planck Society, and intramural funds at TIFR Hyderabad from the Department of Atomic Energy (DAE), India, under the Project Identification Number RTI 4007, towards supporting this project.

**REFERENCES**

1. Mayor R & Etienne-Manneville S (2016) The front and rear of collective cell migration. *Nature reviews. Molecular cell biology* 17(2):97-109.
2. Shellard A & Mayor R (2021) Collective durotaxis along a self-generated stiffness gradient in vivo. *Nature* 600(7890):690-694.
3. Pérez-González C*, et al.* (2021) Mechanical compartmentalization of the intestinal organoid enables crypt folding and collective cell migration. *Nat Cell Biol* 23(7):745-757.
4. Boocock D, Hino N, Ruzickova N, Hirashima T, & Hannezo E (2021) Theory of mechanochemical patterning and optimal migration in cell monolayers. *Nature physics* 17(2):267-274.
5. Barriga EH, Franze K, Charras G, & Mayor R (2018) Tissue stiffening coordinates morphogenesis by triggering collective cell migration in vivo. *Nature* 554(7693):523-527.
6. Kawaguchi K, Kageyama R, & Sano M (2017) Topological defects control collective dynamics in neural progenitor cell cultures. *Nature* 545(7654):327-331.
7. Das T*, et al.* (2015) A molecular mechanotransduction pathway regulates collective migration of epithelial cells. *Nat Cell Biol* 17(3):276-+.
8. Brugués A*, et al.* (2014) Forces driving epithelial wound healing. *Nature physics* 10(9):683-690.
9. Ramel D, Wang XB, Laflamme C, Montell DJ, & Emery G (2013) Rab11 regulates cell-cell communication during collective cell movements. *Nat Cell Biol* 15(3):317-324.
10. Cheung KJ, Gabrielson E, Werb Z, & Ewald AJ (2013) Collective invasion in breast cancer requires a conserved basal epithelial program. *Cell* 155(7):1639-1651.
11. Friedl P, Locker J, Sahai E, & Segall JE (2012) Classifying collective cancer cell invasion. *Nat Cell Biol* 14(8):777-783.
12. Tambe DT*, et al.* (2011) Collective cell guidance by cooperative intercellular forces. *Nature materials* 10(6):469-475.
13. Bianco A*, et al.* (2007) Two distinct modes of guidance signalling during collective migration of border cells. *Nature* 448(7151):362-U312.
14. Hayer A*, et al.* (2016) Engulfed cadherin fingers are polarized junctional structures between collectively migrating endothelial cells. *Nat Cell Biol* 18(12):1311-1323.
15. Rorth P (2012) Fellow travellers: emergent properties of collective cell migration. *Embo Rep* 13(11):984-991.
16. Haeger A, Wolf K, Zegers MM, & Friedl P (2015) Collective cell migration: guidance principles and hierarchies. *Trends Cell Biol* 25(9):556-566.

17. Montell DJ, Yoon WH, & Starz-Gaiano M (2012) Group choreography: mechanisms orchestrating the collective movement of border cells. *Nat Rev Mol Cell Bio* 13(10):631-645.
18. Kozyrska K*, et al.* (2022) p53 directs leader cell behavior, migration, and clearance during epithelial repair. *Science (New York, N.Y.)* 375(6581):eabl8876.
19. Vishwakarma M, Spatz JP, & Das T (2020) Mechanobiology of leader-follower dynamics in epithelial cell migration. *Current opinion in cell biology* 66:97-103.
20. Atsuta Y & Takahashi Y (2015) FGF8 coordinates tissue elongation and cell epithelialization during early kidney tubulogenesis. *Development* 142(13):2329-2337.
21. Friedl P & Gilmour D (2009) Collective cell migration in morphogenesis, regeneration and cancer. *Nat Rev Mol Cell Bio* 10(7):445-457.
22. Vilchez Mercedes SA*, et al.* (2021) Decoding leader cells in collective cancer invasion. *Nature reviews. Cancer* 21(9):592-604.
23. Labernadie A*, et al.* (2017) A mechanically active heterotypic E-cadherin/N-cadherin adhesion enables fibroblasts to drive cancer cell invasion. *Nat Cell Biol* 19(3):224-237.
24. Ilina O*, et al.* (2020) Cell-cell adhesion and 3D matrix confinement determine jamming transitions in breast cancer invasion. *Nat Cell Biol* 22(9):1103-1115.
25. Vishwakarma M*, et al.* (2018) Mechanical interactions among followers determine the emergence of leaders in migrating epithelial cell collectives. *Nat Commun* 9.
26. Reffay M*, et al.* (2014) Interplay of RhoA and mechanical forces in collective cell migration driven by leader cells. *Nat Cell Biol* 16(3):217-223.
27. Peglion F, Llense F, & Etienne-Manneville S (2014) Adherens junction treadmilling during collective migration. *Nat Cell Biol* 16(7):639-651.
28. Riahi R*, et al.* (2015) Notch1-Dll4 signalling and mechanical force regulate leader cell formation during collective cell migration. *Nat Commun* 6:6556.
29. Donà E*, et al.* (2013) Directional tissue migration through a self-generated chemokine gradient. *Nature* 503(7475):285-289.
30. Lawrence RE & Zoncu R (2019) The lysosome as a cellular centre for signalling, metabolism and quality control. *Nat Cell Biol* 21(2):133-142.
31. Ballabio A & Bonifacino JS (2020) Lysosomes as dynamic regulators of cell and organismal homeostasis. *Nature reviews. Molecular cell biology* 21(2):101-118.
32. Schiefermeier N*, et al.* (2014) The late endosomal p14-MP1 (LAMTOR2/3) complex regulates focal adhesion dynamics during cell migration. *The Journal of cell biology* 205(4):525-540.
33. Pu J, Guardia CM, Keren-Kaplan T, & Bonifacino JS (2016) Mechanisms and functions of lysosome positioning. *Journal of cell science* 129(23):4329-4339.
34. Bretou M*, et al.* (2017) Lysosome signaling controls the migration of dendritic cells. *Science immunology* 2(16).
35. Wang G*, et al.* (2018) Biomechanical Control of Lysosomal Secretion Via the VAMP7 Hub: A Tug-of-War between VARP and LRRK1. *iScience* 4:127-143.
36. Abreu-Blanco MT, Verboon JM, Liu R, Watts JJ, & Parkhurst SM (2012) Drosophila embryos close epithelial wounds using a combination of cellular protrusions and an actomyosin purse string. *Journal of cell science* 125(Pt 24):5984-5997.
37. Napolitano G & Ballabio A (2016) TFEB at a glance. *Journal of cell science* 129(13):2475-2481.
38. Martina JA, Chen Y, Gucek M, & Puertollano R (2012) MTORC1 functions as a transcriptional regulator of autophagy by preventing nuclear transport of TFEB. *Autophagy* 8(6):903-914.
39. Rosa-Ferreira C & Munro S (2011) Arl8 and SKIP act together to link lysosomes to kinesin-1. *Developmental cell* 21(6):1171-1178.

40. Heuser J (1989) Changes in lysosome shape and distribution correlated with changes in cytoplasmic pH. *The Journal of cell biology* 108(3):855-864.
41. Guardia CM*, et al.* (2019) Reversible association with motor proteins (RAMP): A streptavidin-based method to manipulate organelle positioning. *PLoS biology* 17(5):e3000279.
42. Balasubramaniam L*, et al.* (2021) Investigating the nature of active forces in tissues reveals how contractile cells can form extensile monolayers. *Nature materials* 20(8):1156-1166.
43. Weber GF, Bjerke MA, & DeSimone DW (2012) A mechanoresponsive cadherin-keratin complex directs polarized protrusive behavior and collective cell migration. *Developmental cell* 22(1):104-115.
44. Zimmermann J, Camley BA, Rappel WJ, & Levine H (2016) Contact inhibition of locomotion determines cell-cell and cell-substrate forces in tissues. *Proceedings of the National Academy of Sciences of the United States of America* 113(10):2660-2665.
45. Valon L, Marín-Llauradó A, Wyatt T, Charras G, & Trepat X (2017) Optogenetic control of cellular forces and mechanotransduction. *Nat Commun* 8:14396.
46. Ravasio A*, et al.* (2015) Gap geometry dictates epithelial closure efficiency. *Nat Commun* 6:7683.
47. Rausch S*, et al.* (2013) Polarizing cytoskeletal tension to induce leader cell formation during collective cell migration. *Biointerphases* 8(1):32.
48. Chen T*, et al.* (2019) Large-scale curvature sensing by directional actin flow drives cellular migration mode switching. *Nature physics* 15:393-402.
49. Machacek M*, et al.* (2009) Coordination of Rho GTPase activities during cell protrusion. *Nature* 461(7260):99-103.
50. Ruth ES (1911) CICATRIZATION OF WOUNDS IN VITRO. *The Journal of experimental medicine* 13(4):422-424.
51. Remorino A*, et al.* (2017) Gradients of Rac1 Nanoclusters Support Spatial Patterns of Rac1 Signaling. *Cell reports* 21(7):1922-1935.
52. Fritz RD & Pertz O (2016) The dynamics of spatio-temporal Rho GTPase signaling: formation of signaling patterns. *F1000Research* 5.
53. Palamidessi A*, et al.* (2008) Endocytic trafficking of Rac is required for the spatial restriction of signaling in cell migration. *Cell* 134(1):135-147.
54. Valentin G, Haas P, & Gilmour D (2007) The chemokine SDF1a coordinates tissue migration through the spatially restricted activation of Cxcr7 and Cxcr4b. *Current biology : CB* 17(12):1026-1031.
55. Monteleon CL*, et al.* (2018) Lysosomes Support the Degradation, Signaling, and Mitochondrial Metabolism Necessary for Human Epidermal Differentiation. *The Journal of investigative dermatology* 138(9):1945-1954.
56. Juarez MT, Patterson RA, Li W, & McGinnis W (2013) Microinjection wound assay and in vivo localization of epidermal wound response reporters in Drosophila embryos. *Journal of visualized experiments : JoVE* (81):e50750.
57. Narasimha M & Brown NH (2006) Chapter 8 - Confocal Microscopy of Drosophilia Embryos. *Cell Biology (Third Edition)*, ed Celis JE (Academic Press, Burlington), pp 77-86.

Figure 1

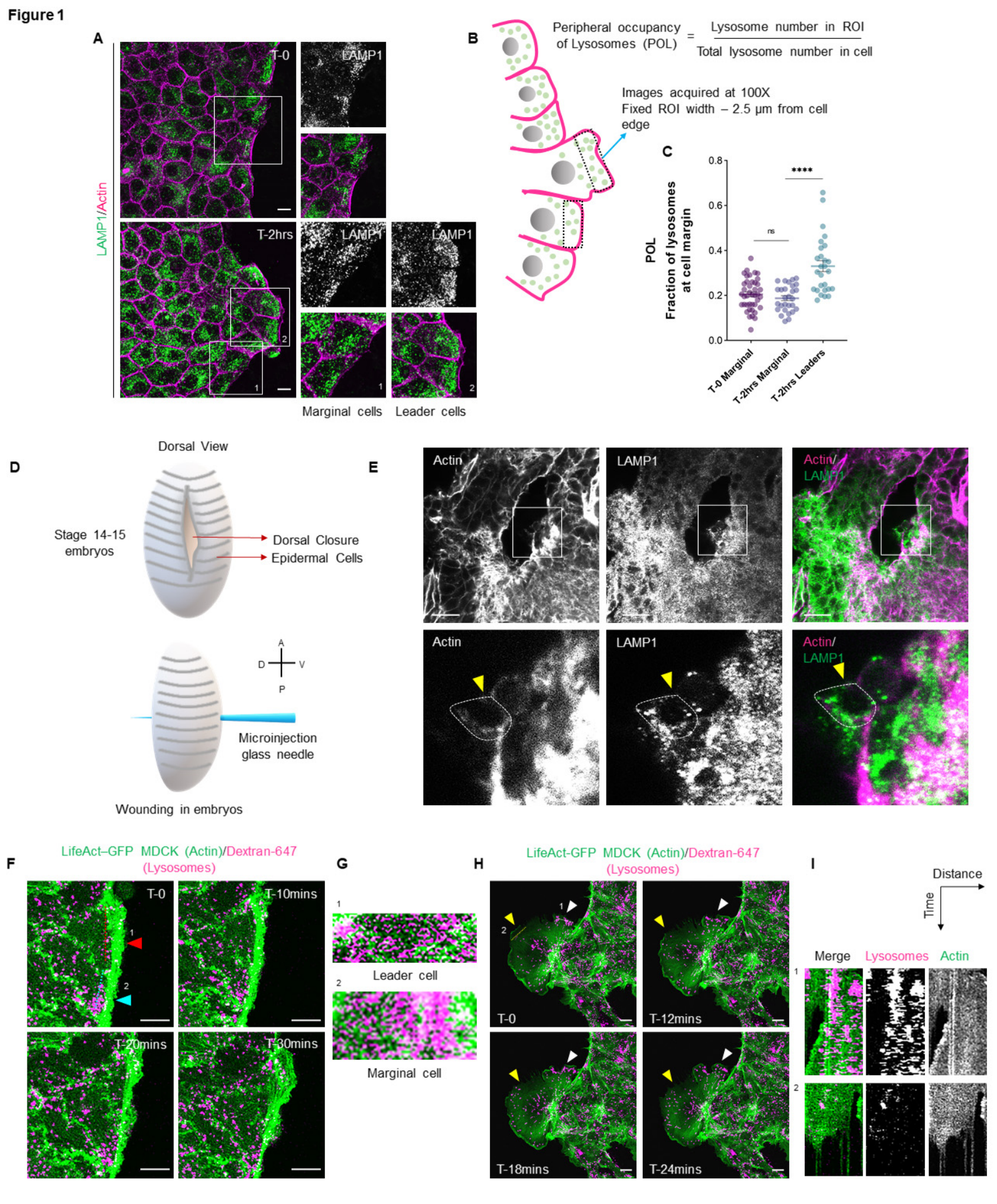
A
LAMP1/Actin
T-0
LAMP1
T-2hrs
LAMP1
LAMP1
Marginal cells
Leader cells
B
Peripheral occupancy of Lysosomes (POL) = Lysosome number in ROI / Total lysosome number in cell
Images acquired at 100X
Fixed ROI width – 2.5 µm from cell edge
C
POL
Fraction of lysosomes at cell margin
0.8
0.6
0.4
0.2
0.0
ns
****
T-0 Marginal
T-2hrs Marginal
T-2hrs Leaders
D
Dorsal View
Stage 14-15 embryos
Dorsal Closure
Epidermal Cells
A
D
V
P
Microinjection glass needle
Wounding in embryos
E
Actin
LAMP1
Actin/ LAMP1
F
LifeAct–GFP MDCK (Actin)/Dextran-647 (Lysosomes)
T-0
T-10mins
T-20mins
T-30mins
G
Leader cell
Marginal cell
H
LifeAct-GFP MDCK (Actin)/Dextran-647 (Lysosomes)
T-0
T-12mins
T-18mins
T-24mins
I
Distance
Time
Merge
Lysosomes
Actin

Figure 2

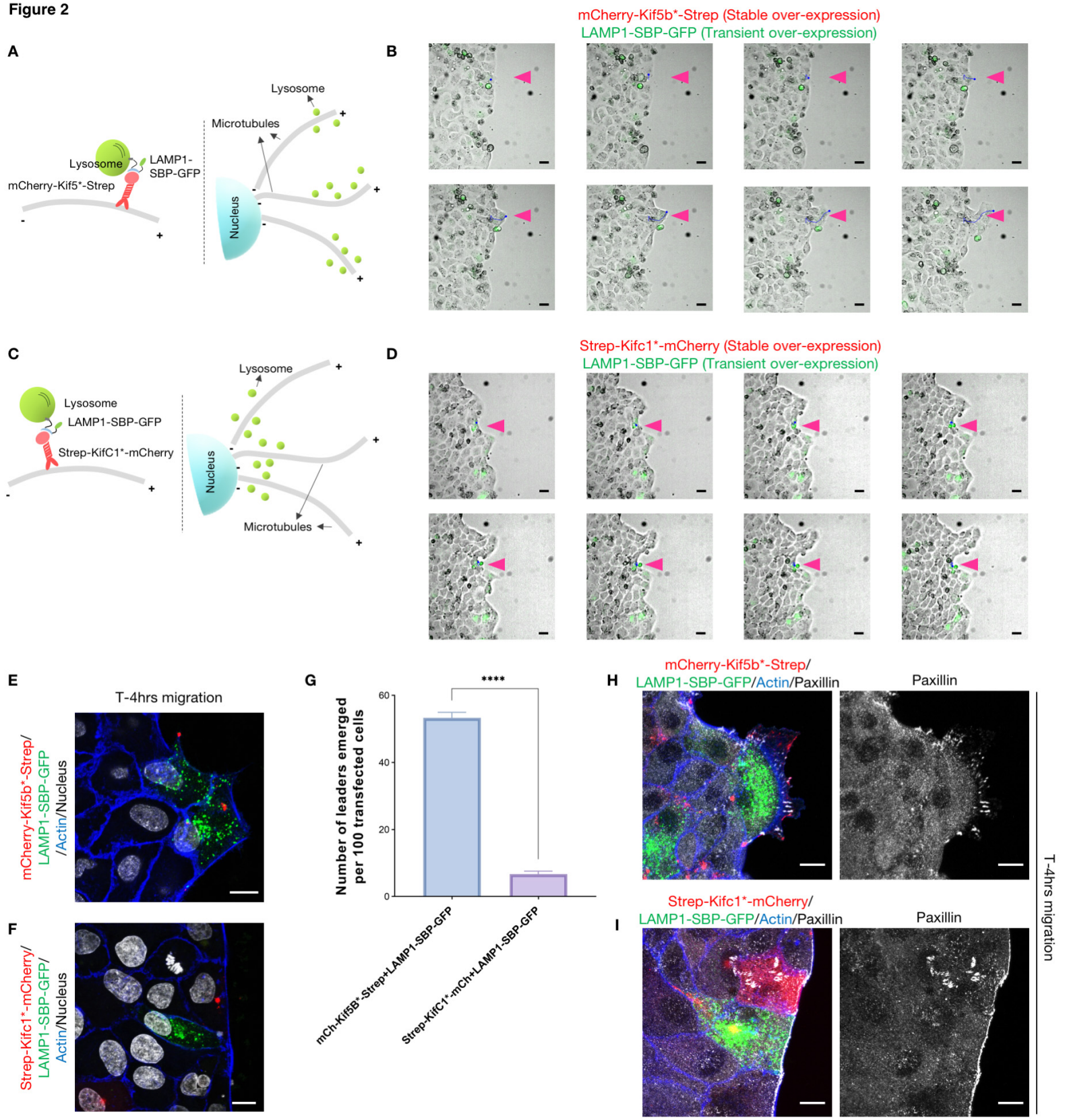
A
Lysosome
LAMP1-SBP-GFP
mCherry-Kif5*-Strep
Microtubules
Nucleus
B
mCherry-Kif5b*-Strep (Stable over-expression)
LAMP1-SBP-GFP (Transient over-expression)
C
Lysosome
LAMP1-SBP-GFP
Strep-KifC1*-mCherry
Nucleus
Microtubules
D
Strep-Kifc1*-mCherry (Stable over-expression)
LAMP1-SBP-GFP (Transient over-expression)
E
T-4hrs migration
mCherry-Kif5b*-Strep/
LAMP1-SBP-GFP
/Actin/Nucleus
F
Strep-Kifc1*-mCherry/
LAMP1-SBP-GFP/
Actin/Nucleus
G
****
Number of leaders emerged per 100 transfected cells
60
40
20
0
mCh-Kif5B*-Strep+LAMP1-SBP-GFP
Strep-KifC1*-mCh+LAMP1-SBP-GFP
H
mCherry-Kif5b*-Strep/
LAMP1-SBP-GFP/Actin/Paxillin
Paxillin
I
Strep-Kifc1*-mCherry/
LAMP1-SBP-GFP/Actin/Paxillin
Paxillin
T-4hrs migration

Figure 3

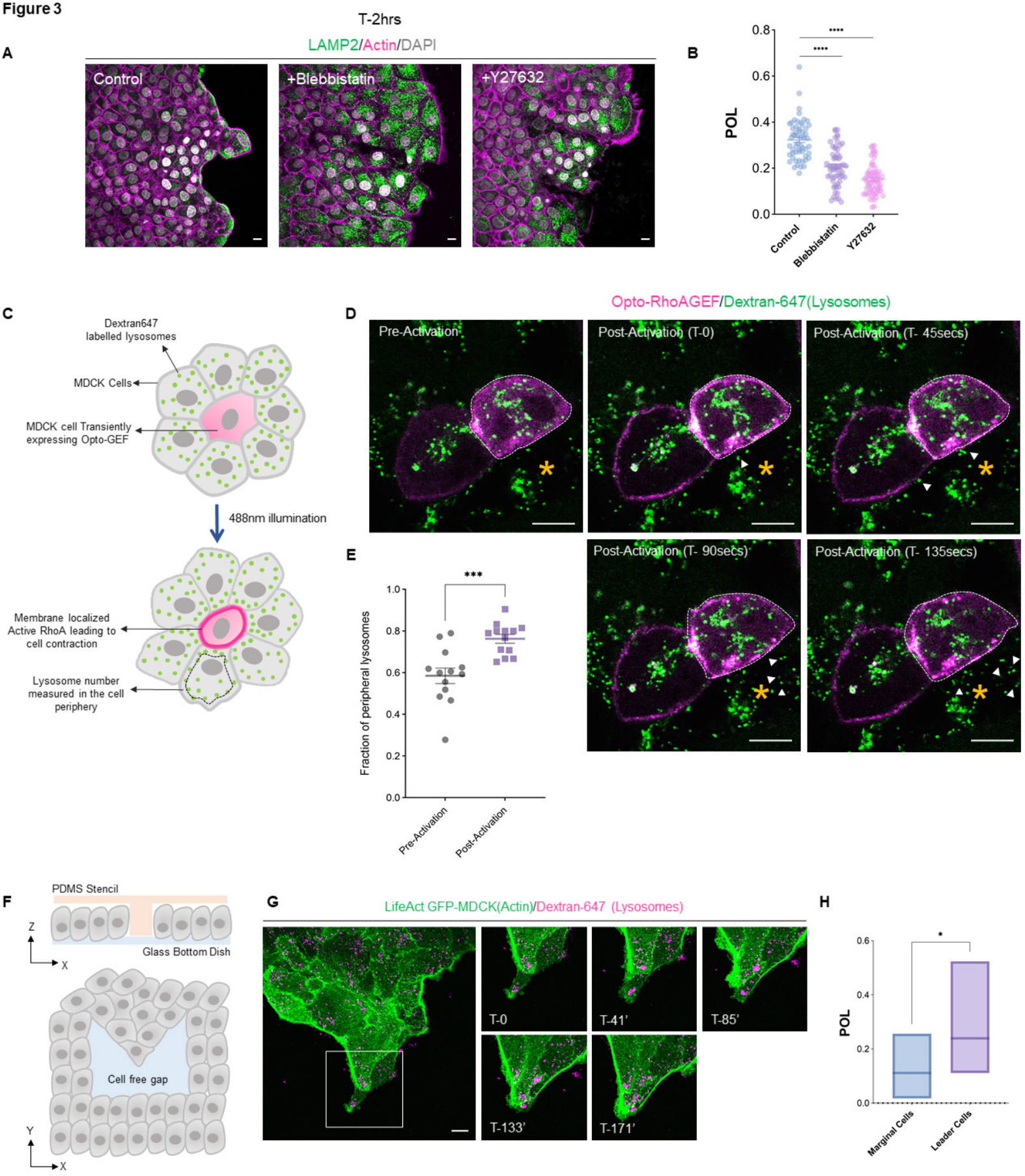
T-2hrs
A
LAMP2/Actin/DAPI
Control
+Blebbistatin
+Y27632
B
POL
0.8
0.6
0.4
0.2
0.0
****
****
Control
Blebbistatin
Y27632
C
Dextran647 labelled lysosomes
MDCK Cells
MDCK cell Transiently expressing Opto-GEF
488nm illumination
Membrane localized Active RhoA leading to cell contraction
Lysosome number measured in the cell periphery
D
Opto-RhoAGEF/Dextran-647(Lysosomes)
Pre-Activation
Post-Activation (T-0)
Post-Activation (T- 45secs)
Post-Activation (T- 90secs)
Post-Activation (T- 135secs)
E
Fraction of peripheral lysosomes
1.0
0.8
0.6
0.4
0.2
0.0
***
Pre-Activation
Post-Activation
F
PDMS Stencil
Z
X
Glass Bottom Dish
Cell free gap
Y
X
G
LifeAct GFP-MDCK(Actin)/Dextran-647 (Lysosomes)
T-0
T-41'
T-85'
T-133'
T-171'
H
POL
0.6
0.4
0.2
0.0
*
Marginal Cells
Leader Cells

Figure 4

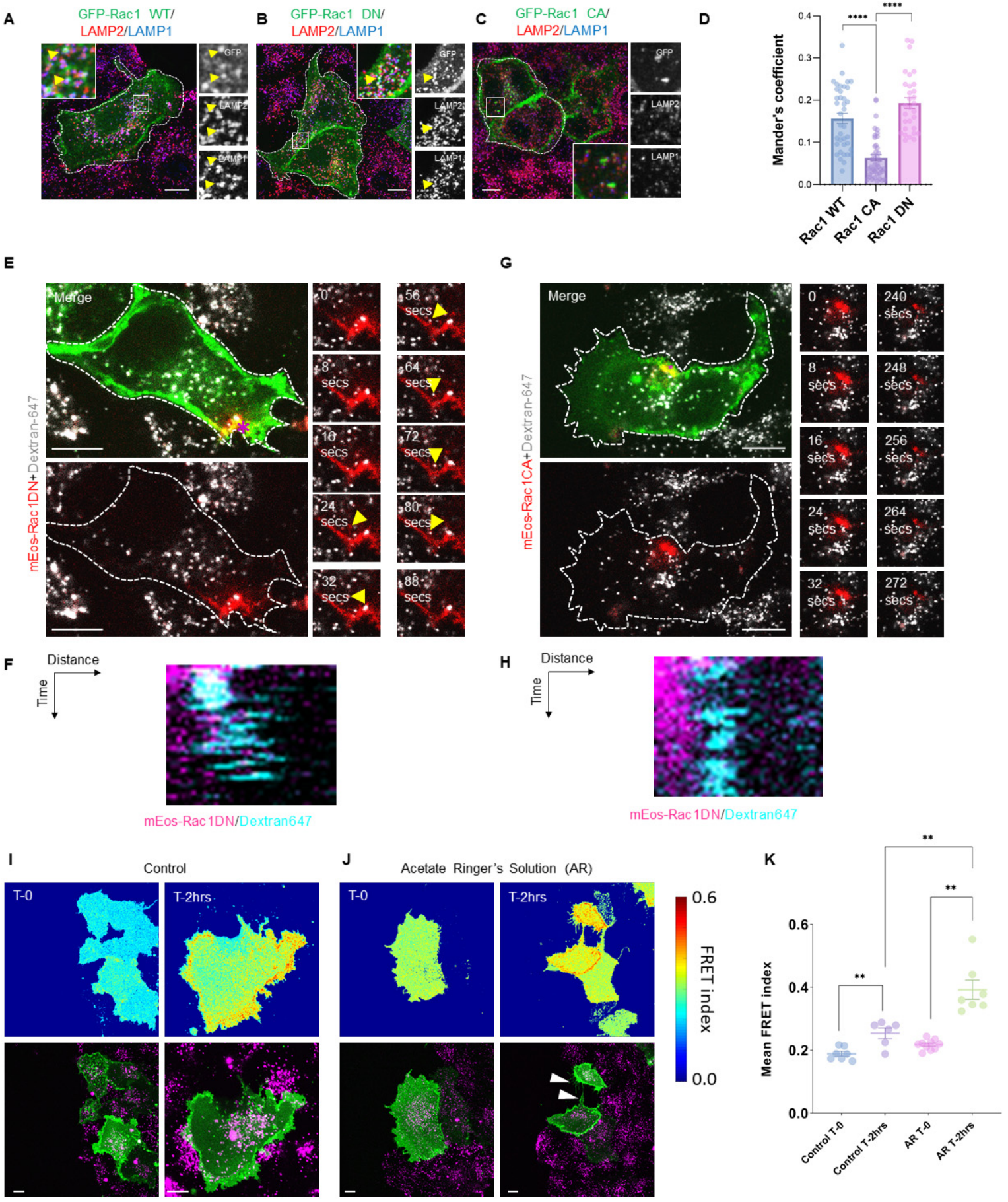
A
GFP-Rac1 WT/
LAMP2/LAMP1
GFP
LAMP2
LAMP1
B
GFP-Rac1 DN/
LAMP2/LAMP1
C
GFP-Rac1 CA/
LAMP2/LAMP1
D
Mander's coefficient
0.0
0.1
0.2
0.3
0.4
*
****
****
Rac1 WT
Rac1 CA
Rac1 DN
E
Merge
mEos-Rac1DN+Dextran-647
0
8 secs
16 secs
24 secs
32 secs
56 secs
64 secs
72 secs
80 secs
88 secs
G
Merge
mEos-Rac1CA+Dextran-647
0
8 secs
16 secs
24 secs
32 secs
240 secs
248 secs
256 secs
264 secs
272 secs
F
Distance
Time
mEos-Rac1DN/Dextran647
H
Distance
Time
mEos-Rac1DN/Dextran647
I
Control
T-0
T-2hrs
J
Acetate Ringer's Solution (AR)
T-0
T-2hrs
0.6
FRET index
0.0
K
Mean FRET index
0.0
0.2
0.4
0.6
**
**
**
Control T-0
Control T-2hrs
AR T-0
AR T-2hrs

**Figure 5**

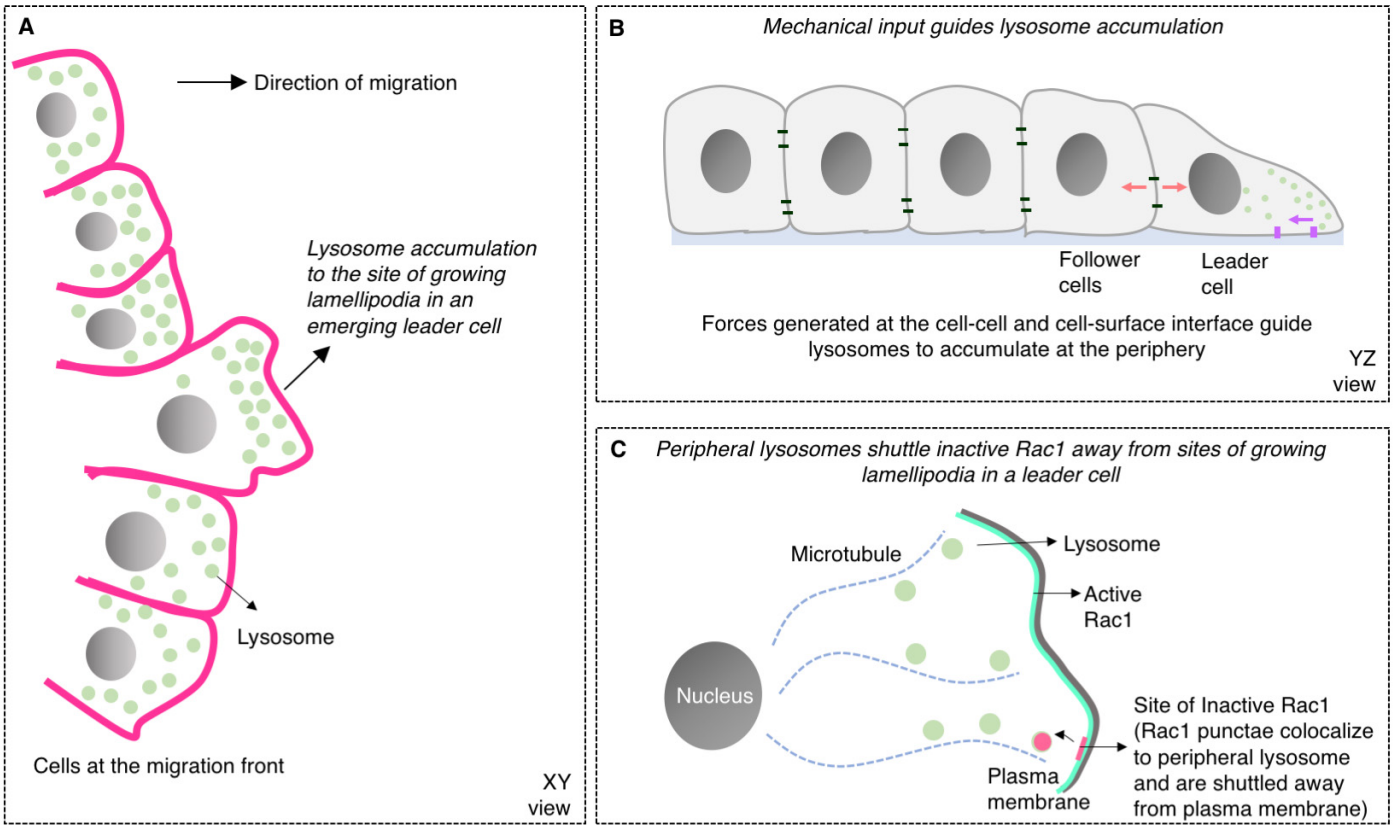
A
Direction of migration
Lysosome accumulation to the site of growing lamellipodia in an emerging leader cell
Lysosome
Cells at the migration front
XY view
B
Mechanical input guides lysosome accumulation
Follower cells
Leader cell
Forces generated at the cell-cell and cell-surface interface guide lysosomes to accumulate at the periphery
YZ view
C
Peripheral lysosomes shuttle inactive Rac1 away from sites of growing lamellipodia in a leader cell
Microtubule
Lysosome
Active Rac1
Nucleus
Site of Inactive Rac1 (Rac1 punctae colocalize to peripheral lysosome and are shuttled away from plasma membrane)
Plasma membrane